Slowness curves and characteristics of surface acoustic waves propagating obliquely in periodic finite-thickness electrode gratings

Vincent Laude[a)] and Sylvain Ballandras

Laboratoire de Physique et de Métrologie des Oscillateurs, CNRS UPR 3203,
associé à l'Université de Franche-Comté, 32 avenue de l'Observatoire, F-25044 Besançon, France

The computation of the diffraction of surface acoustic waves (SAWs) on piezoelectric materials is complicated by the anisotropy of their propagation, and requires their slowness curves to be known precisely. In addition, in actual devices these slowness curves are strongly affected by the massive electrodes used for SAW generation. We investigate the characteristics of SAWs propagating obliquely in periodic finite-thickness electrode gratings, with the mass-loading effect taken into account. The velocity of the surface waves, as well as the attenuation, piezoelectric coupling and beam steering are obtained as a function of the propagation angle with respect to the grating axis. The slowness curves for SAWs propagating under periodic electrode gratings are compared with the slowness curves for the same SAWs propagating under a thick homogeneous metallic layer. Numerical examples are presented for the SAWs of 42.75°YX quartz and X112.2°Y lithium tantalate, and the leaky SAWs of 36°YX lithium tantalate. © *2003 American Institute of Physics.* [DOI: 10.1063/1.1582237]

I. INTRODUCTION

During the last decade, much work has been devoted to the modeling and the numerical simulation of surface acoustic waves (SAWs) propagating under interdigital transducers, including the mass-loading effect. This effort was especially useful to understand the wave propagation characteristics in actual SAW filters and devices, and hence are now used routinely to obtain the basic parameters required for filter design. Although a pure finite element analysis (FEA) is possible,[1,2] most approaches are based on a mixed FEA/ boundary integral method (BIM),[3–6] in which the wave solution in the electrodes and in the substrate are respectively obtained by FEA and a Green's function integral solution, and the two domains are related using a BIM to obtain the strip or harmonic admittance. One limitation of the FEA/ BIM method is that for computational reasons the problem is generally restricted to two dimensions, with the electrodes assumed infinite in the transverse direction. However, real SAW devices are of finite width, and transverse effects occur that cannot be taken into account using a two-dimensional model. Though an exact three dimensional model for filter design is probably still beyond reach, useful information can be gained by examining the propagation of slanted acoustic waves in periodic gratings. Indeed, diffraction effects caused by the finite transverse dimension of the electrodes can in principle be addressed by developing the transverse wave structure using the angular spectrum of waves formalism, i.e., as a sum over slanted acoustic waves.[7] Such an approach requires their slowness curves to be known precisely.

Hashimoto *et al.*[8] have addressed the problem of computing the strip admittance for slanted SAWs propagating in finite-thickness electrode gratings, and have obtained dispersion relations for a given propagation direction. In this article, we address the problem of obtaining the slowness curves for surface acoustic waves propagating in periodic finite-thickness electrode gratings. Defining θ as the angle of propagation with respect to the electrodes' axis, we show how the phase velocity can be obtained as a function of θ, including the mass-loading effect, using the harmonic admittance (HA) approach.[6,9] We discuss the way the HA computation has to be modified to accommodate for slanted propagation, and especially the finite element model we have used. The assumptions in this model and their validity range are discussed. Along with the phase velocity, we also discuss how other useful information regarding the propagating waves can be obtained as a function of the propagation angle, i.e., the attenuation, the electro-mechanical coupling, the beam-steering angle and its derivative. This derivative, known as the diffraction parameter, is a measure of the importance of diffraction in a given propagation direction. Numerical simulation results are presented for standard piezoelectric substrates widely used for the fabrication of SAW devices, i.e., 42.75°YX quartz and X112.2°Y lithium tantalate (true SAW), and 36°YX lithium tantalate (pseudo or leaky SAW). The slowness curves for SAWs propagating under periodic electrode gratings are compared with slowness curves for the same SAWs propagating under a thick homogeneous metallic layer. The results are discussed according to the nature of the surface wave, and the slowness curves are shown to be strongly dependent on the thickness of the electrodes.

II. SLOWNESS CURVES

We consider SAW propagation in the (x_1, x_3) plane, as depicted in Fig. 1. Axis x_2 is then normal to the substrate,

---

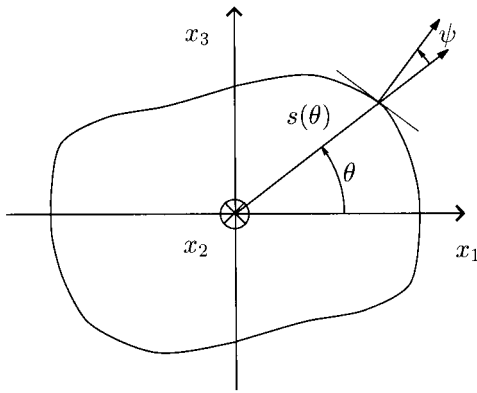[a)]Author to whom correspondence should be addressed; electronic mail: vincent.laude@lpmo.edu

FIG. 1. Slowness curve definitions.

FIG. 2. Geometry for slanted SAW propagation in a periodic metallic grating.

and directed inward. We first discuss here how the knowledge of the slowness dependence on the propagation angle can be exploited to obtain the beam-steering and the diffraction parameter in a periodic electrode grating. In the case of a free or shorted surface, and also in the case of a uniform metallic layer deposited on the piezoelectric substrate, the beam steering is best obtained by directly computing the Poynting vector, which is known to be normal to the slowness curve. In the case of propagation in a periodic electrode grating, it is more practical to numerically differentiate the slowness curve. Let us assume that we can compute the slowness as a function of the propagation angle, i.e., the function $s(\theta)$ in polar coordinates is known, with the angle θ expressed in radians. The coordinates of a running point on the slowness curve, as shown on Fig. 1, is then

$$\begin{pmatrix} x(\theta) \\ y(\theta) \end{pmatrix} = \begin{pmatrix} s(\theta)\cos(\theta) \\ s(\theta)\sin(\theta) \end{pmatrix}, \tag{1}$$

from which the tangent at that point is

$$\begin{pmatrix} x'(\theta) \\ y'(\theta) \end{pmatrix} = \begin{pmatrix} s'(\theta)\cos(\theta) - s(\theta)\sin(\theta) \\ s'(\theta)\sin(\theta) + s(\theta)\cos(\theta) \end{pmatrix}. \tag{2}$$

The beam steering, or power-flow, angle ψ is defined as the angle between the normal to the slowness curve and the phase direction. Expressing this condition and after some simple algebra, we arrive at

$$\begin{pmatrix} \cos\psi \\ \sin\psi \end{pmatrix} = \frac{1}{d(\theta)} \begin{pmatrix} 1 \\ -g(\theta) \end{pmatrix} \tag{3}$$

with the definitions

$$g(\theta) = \frac{d}{d\theta}\log s(\theta) = \frac{s'(\theta)}{s(\theta)} \tag{4}$$

and

$$d(\theta) = \sqrt{1 + g^2(\theta)}. \tag{5}$$

From Eqs. (3)–(5), the beam-steering angle can be computed by evaluating the first derivative of the slowness curve. By definition, the diffraction parameter is

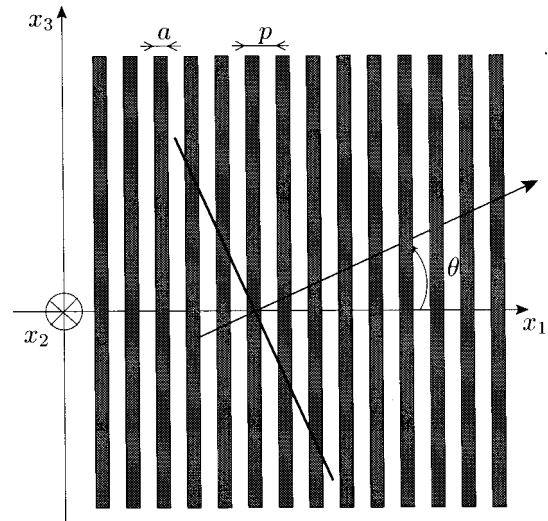$$\Gamma(\theta) = \frac{d\psi(\theta)}{d\theta}. \tag{6}$$

Since the beam-steering angle is obtained as a first derivative, the diffraction parameter is obtained as a second derivative of the slowness curve, and can be expressed as

$$\Gamma(\theta) = \frac{-g'(\theta)}{1 + g^2(\theta)}. \tag{7}$$

The derivation in this section is indeed elementary, and similar expressions can be found in the literature.[10] However, our derivation does not rely on any approximation such as the parabolic approximation often used in the diffraction theory of SAWs.

III. ESTIMATION OF SAW PARAMETERS

In the process of computing slowness curves for surface waves, it is necessary to locate the slowness as a function of the propagation angle θ in the surface plane. The actual algorithm employed will depend on the nature of the propagation problem. On a free or shorted surface, the wave characteristics are functions of the material constants only, and are not dispersive. Under a metallic grating, however, the wave characteristics are dispersive. Figure 2 illustrates the notations used for describing the electrode grating. The grating is periodic with period p. The width and height of the electrodes are denoted a and h, respectively. Because of the periodicity, the wave characteristics depend on the frequency period product fp and on the metallization ratio a/p, but in addition they also depend on the electrode's shape, which for a rectangular electrode is scaled by the form factor $h/(2p)$. A metallization ratio of 0.5 is assumed for all computations, but of course the value of this coefficient may influence the results. For propagation under a thick metallic layer deposited upon the piezoelectric substrate, the wave characteristics are also dispersive, and depend on the frequency thickness product fh, where h is now understood as the layer thickness.

In the case of a homogeneous surface with either free or shorted boundary conditions, it is well known that the slowness is given, respectively, by a zero or a pole of the so-

called effective permittivity. Such an approach has been used routinely to obtain maps of surface wave parameters.[11] The effective permittivity is a restriction of the Green's function of the semi-infinite substrate to its electrical components.[9] The practical computation of the surface Green's function in the spectral domain has, for instance, been described in Ref. 12.

In the case of periodic electrode gratings, two additional phenomena have to be accounted for, namely the frequency dependence arising from the periodic perturbation of the surface and the periodic electrical excitation of waves along axis x_1, and the so-called mass-loading effect of the electrodes. The first phenomenon is adequately described (at least as regards the electrical part of the problem) using the notion of the strip admittance,[13] extended to the notion of harmonic admittance in Ref. 9. The occurrence of a piezoelectrically coupled surface wave is then given by a pole of the HA. There have been many approaches to the computation of the mass-loading effect, with most of them relying on a FEA of the acoustical propagation in the electrodes.[2–6] In this work, we have used the approach described in Ref. 6, which is a combination of a FEA for the electrodes with a BIM relying upon the Green's function of the semi-infinite substrate. For the practical computation of the HA we have enriched the original software described in Ref. 6. One improvement is the computation of spectral Green's function as a function of slownesses s_1 and s_3 instead of assuming $s_3 = 0$ as was originally done. Our procedure for computing the spectral Green's function is similar to the one described by Peach in Ref. 12. A second improvement is the definition of a special finite element suited to the problem considered. We describe in the next section how the classical finite element approach can be modified to accommodate for slanted propagation.

One difficulty arising with the propagation of a slanted surface acoustic wave in an electrode grating is the requirement that the potential satisfies a $V \exp(-jk_3x_3)$ transverse dependence, for an assigned transverse slowness s_3 and transverse wave vector $k_3 = 2\pi f s_3$.[8] Indeed, in the frame of the quasistatic approximation, one would expect the potential along any ideally conducting electrode to have a unique value at any time. The model considered in this work can indeed be viewed as describing two different physical problems. First, as we argued in the introduction, the operation of a finite width SAW transducer can be modeled using the angular spectrum of waves approach, in which case the electrical excitation is expanded in Fourier components along the transverse direction. It is then possible to consider the solution for each of these Fourier components, which have a $V(k_3)\exp(-jk_3x_3)$ transverse dependence. Obviously, only the superposition of these elementary solutions can be considered as having a physical existence, and it will satisfy the quasistatic approximation by construction. Stated differently, the superposition will satisfy the boundary condition of zero tangential field in the region of the electrodes while the elementary Fourier components will not. Second, our model also physically describes the propagation of a slanted SAW under a shorted electrode grating, but rigorously only at resonance. By resonance, we mean that conditions, i.e., slowness

as a function of frequency and grating parameters, for which a pole in the HA is obtained. For, in this case, charges exist under the electrodes although the potential vanishes on them ($V=0$). Then the boundary condition of zero tangential field in the region of the electrodes will be satisfied while at the same time all other fields, i.e., mechanical displacements, stresses and electric displacement, will have a $\exp(-jk_3x_3)$ transverse dependence.

We next describe how the SAW parameters are estimated from the HA. It has been shown[9] that the contribution of a SAW to the HA takes the following approximate form:

$$Y_s(\gamma) = \frac{jY_0}{\tan(\phi_s/2)} \frac{1-\cos(2\pi\gamma)}{\cos(\phi_s)-\cos(2\pi\gamma)}, \qquad (8)$$

where γ is the driving parameter of the harmonic excitation potential, which on electrode number n is imposed to be

$$V_n(\gamma,x_3) = V_0 \exp(-2j\pi n\gamma)\exp(-jk_3x_3). \qquad (9)$$

Note that the transverse harmonic dependence $\exp(-jk_3x_3)$ in the excitation potential also appears in the expression of the currents that are created by charges under the electrodes, and thus does not appear in the expression of the HA, since an admittance is a current to potential ratio. In Eq. (8), ϕ_s is the phase delay per grating period, from which the slowness at resonance is estimated as

$$\hat{s} = \frac{\phi_s}{2\pi fp}. \qquad (10)$$

The attenuation can also be estimated via Eq. (10) if the phase delay is considered complex. Note that the HA, and hence parameters ϕ_s and Y_0, are implicitly dependent on the parameters fp, s_3, a/p, and $h/2p$. The static capacitance contribution to the HA is taken to be of the form[9]

$$Y_c(\gamma) = C \sin(\pi|\gamma|) \qquad (11)$$

and the total HA is modeled for the estimation process as the sum

$$Y_e(\gamma,fp) = Y_s(\gamma) + Y_c(\gamma). \qquad (12)$$

Thereby the contribution of bulk waves is neglected in the estimation of the parameters, although it is naturally included in the FEA/BIM computation. The unknown parameters ϕ_s, Y_0 and C are estimated via a mean squares fit of the model of Eq. (12) to the numerical simulation of the HA obtained using the extended FEA/BIM method. Most quantities that can be estimated are rather well defined, i.e., the velocity at resonance (the inverse of the slowness), the attenuation, the beam-steering angle and the diffraction parameter, but this is not true for the coupling strength. It is customary to employ the K^2 definition for this purpose, however this is defined solely for propagation on either a free or a shorted surface, and is moreover adequate only for a lossless SAW, i.e., it does not apply to a leaky SAW.[9,14] The coupling strength used to plot Figs. 6, 10 and 14 is the ratio Y_0/C, and should be considered to have a relative significance only. In an equivalent electrical circuit representation, this quantity would be understood as the ratio of the motional capacitance to the static capacitance.

As will be shown in the next section, the result of the FEA depends on both the frequency period product fp and the transverse slowness s_3. The Green's functions appearing in the BIM are dependent on s_1 and s_3; γ in Eqs. (8)–(12) is related to s_1 by the relation $\gamma = fps_1$ modulo 1. When generating a slowness curve at fixed fp, it would be incorrect to set the value of s_3 and to search for a value of s_1 corresponding to a pole of the HA; although the position of the pole would be correctly located, the remaining parameters would not be correctly estimated. Instead, the propagation angle θ should be considered a constant, and the search should be upon the slowness s defined by

$$s_1 = s \cos \theta; \quad s_3 = s \sin \theta. \tag{13}$$

We emphasize that the slowness that is determined using the method described in this article is the slowness at resonance, i.e., the slowness of the pole of the HA, and is not properly speaking the slowness of the SAW in the grating since it includes reflection effects. It is well known that if there are no reflections on the electrodes then these two slowness' are equal, but that if reflections are not negligible then the slowness of the resonance pole is shifted.[15]

IV. FINITE ELEMENT FOR SLANTED PROPAGATION

The finite element that we use was derived from a classical two-dimensional triangle with 3 degrees of freedom, originally intended for isotropic acoustic problems. More precisely, for an infinitely long electrode, the displacements and constraints are usually assumed not to depend on the transverse coordinate x_3 (hence the two-dimensional element), but the three components of the displacement must be taken into account (hence the 3 degrees of freedom). Another possible representation of the finite element is an infinitely long cylinder with a triangular section. To take into account slanted propagation inside the electrodes, we assume in addition a sinusoidal dependence of the displacements on the transverse coordinate with a given wave-vector component $k_3 = 2\pi f s_3$ according to

$$\mathbf{u} = \sin(k_3 x_3 + \varphi)[P(x_1, x_2)]\{\mathbf{u}\}_T, \tag{14}$$

where φ is an arbitrary phase, T stands for the finite element considered, P is the polynomial interpolation inside the element, and $\{\mathbf{u}\}_T$ is the vector of the nodal values of the displacement field. It is worth noting that the arbitrary angle φ needs not be the same for all components of the displacements; it will, however, drop in the formulation of the FEA. Following the usual procedure of FEA, a variational problem is constructed, which can be given the following linear form:[16]

$$([K] - \omega^2[M])\{\mathbf{u}\} = \{\mathbf{B}\}, \tag{15}$$

where K is the stiffness matrix, M is the mass matrix, $\omega = 2\pi f$ is the angular frequency and $\{\mathbf{B}\}$ represents the excitation forces applied to the nodes. Using the notations $[P]$ for the polynomial interpolation matrix, $[DP]$ for the matrix of the polynomial derivatives, $[C]$ for the stiffness tensor in contracted notation, ρ for the mass density, and the constant matrices

$$[D] = \begin{vmatrix} 1 & 0 & 0 & 0 & 0 & 0 \\ 0 & 0 & 0 & 1 & 0 & 0 \\ 0 & 0 & 0 & 0 & 0 & 0 \\ 0 & 1 & 1 & 0 & 0 & 0 \\ 0 & 0 & 0 & 0 & 0 & 1 \\ 0 & 0 & 0 & 0 & 1 & 0 \end{vmatrix} \tag{16}$$

and

$$[D_3] = \begin{vmatrix} 0 & 0 & 0 \\ 0 & 0 & 0 \\ 0 & 0 & 1 \\ 0 & 0 & 0 \\ 0 & 1 & 0 \\ 1 & 0 & 0 \end{vmatrix} \tag{17}$$

the elementary stiffness and mass matrices[16] can be written, respectively, as

$$[M_T] = \int_T [P]^t \rho [P] d\mathbf{x} \tag{18}$$

and

$$[K_T] = \begin{aligned} &\int_T ([D][DP])^t [C]([D][DP]) d\mathbf{x} \\ &+ k_3^2 \int_T ([D_3][P])^t [C]([D_3][P]) d\mathbf{x}, \end{aligned} \tag{19}$$

where the upper-script t stands for matrix transposition. In the derivation, the sinusoidal dependence has dropped by integration along the x_3 axis, together with the dependence on the phase origin φ. By comparison with the usual case of normal propagation, $k_3 = 0$, it is seen that only the stiffness matrix is affected, and that a positive matrix has to be added
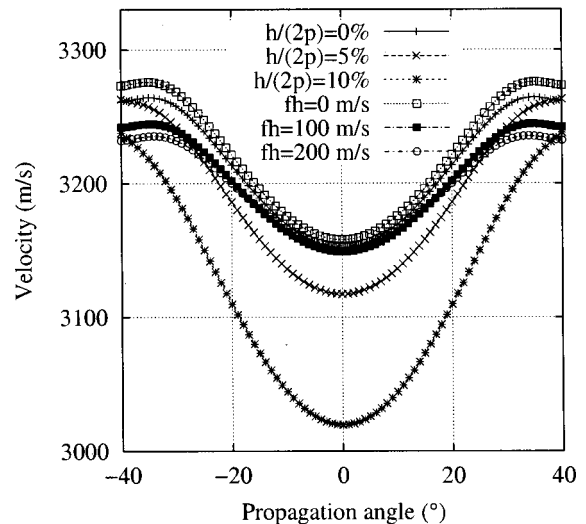

FIG. 3. Velocity of the SAW of 42.75°YX quartz under an aluminum layer for some values of fh, and in a periodic grating with $fp = 1000$ m/s, $a/p = 0.5$ and for some values of $h/(2p)$; f is the frequency, p the period, a the width, and h the thickness.
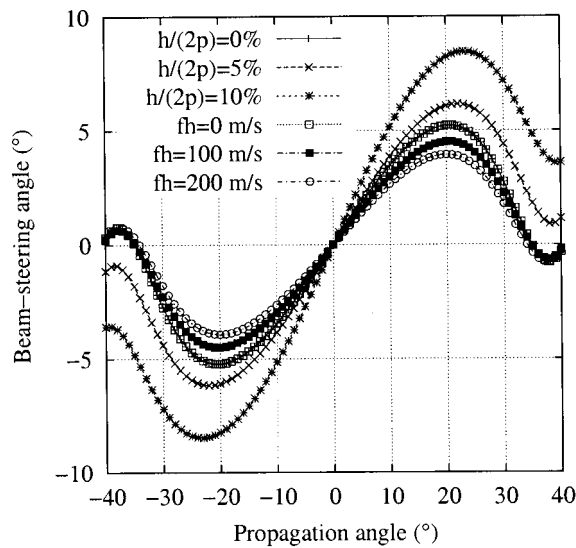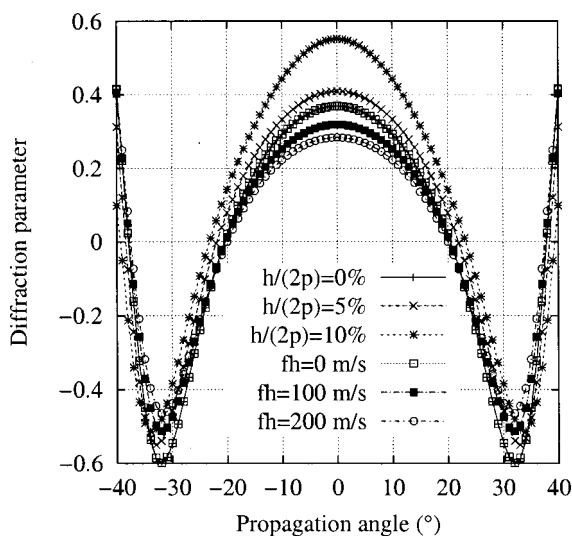
FIG. 4. Beam steering of the SAW of 42.75°YX quartz under an aluminum layer for some values of fh, and in a periodic grating with $fp = 1000$ m/s, $a/p = 0.5$ and for some values of $h/(2p)$.
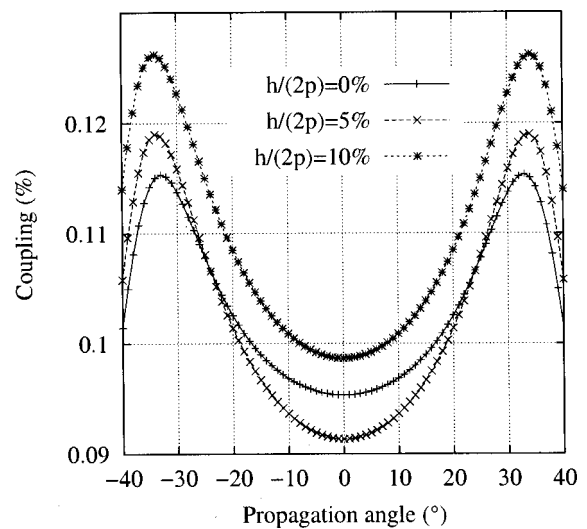
FIG. 6. Coupling strength of the SAW of 42.75°YX quartz in a periodic grating with $fp = 1000$ m/s, $a/p = 0.5$ and for some values of $h/(2p)$.

to it, weighted by the square of the transverse wave vector. In particular, it is seen that terms proportional to the first power of k_3 vanish. Physically, this is supported by the fact that since propagation is isotropic inside the electrode, the solution must be symmetric with respect to $k_3 = 0$. Mathematically, this guarantees that the stiffness matrix retains its positive definite character; otherwise the problem could not be guaranteed to be solvable.

The modified FEA is then used to compute the relation between the displacements and the stress components normal to the electrode-substrate interface, following the method of Ref. 6, but with the extra dependence on k_3 included.

V. SIMULATION EXAMPLES

All results presented in this section are obtained for an infinite periodic electrode grating on a semi-infinite piezoelectric substrate. The zero propagation angle refers to propagation along the grating axis. All parameters given are those obtained for a pole or pseudo pole of the harmonic admittance, i.e., for the resonance condition, with the frequency period product set to 1000 m/s, i.e., far from the stop band in all cases.

The 42.75°YX cut of quartz considered in Figs. 3–6 is also known as $(YX\ell)/42.75$ in the IEEE 1949 piezoelectric standard.[17] The dependence of the resonance slowness, beam steering, diffraction parameter and piezoelectric coupling for the SAW on this cut are depicted in Figs. 3, 4, 5 and 6, respectively, for three values of the electrode aspect ratio $h/(2p)$ (0%, 5% and 10%). In these figures, we have added
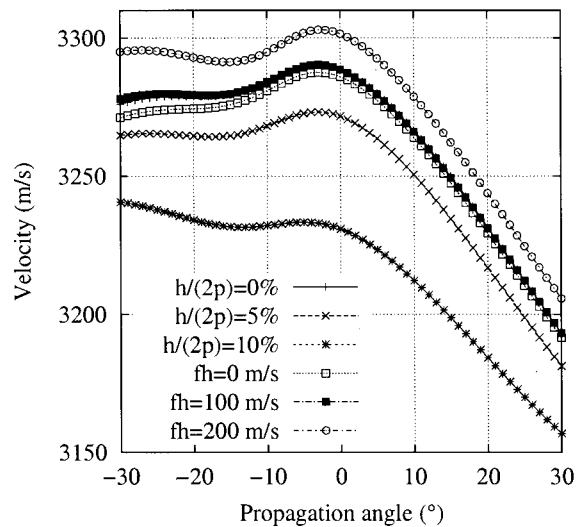
FIG. 5. Diffraction parameter of the SAW of 42.75°YX quartz under an aluminum layer for some values of fh, and in a periodic grating with $fp = 1000$ m/s, $a/p = 0.5$ and for some values of $h/(2p)$.

FIG. 7. Velocity of the SAW of X112°Y lithium tantalate under an aluminum layer for some values of fh, and in a periodic grating with $fp = 1000$ m/s, $a/p = 0.5$ and for some values of $h/(2p)$.
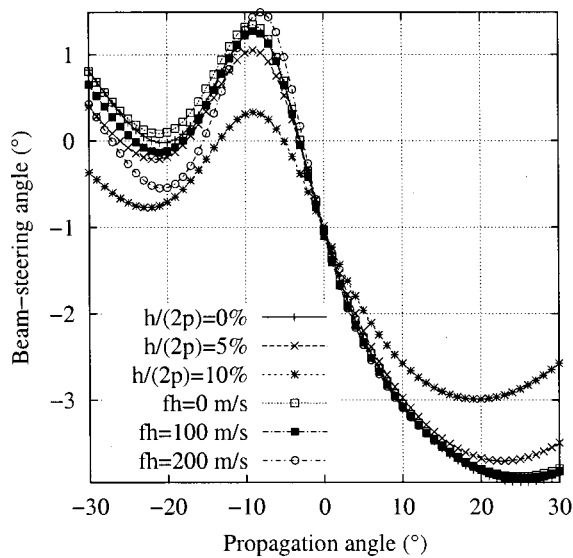
FIG. 8. Beam steering of the SAW of X112°Y lithium tantalate under an aluminum layer for some values of fh, and in a periodic grating with fp = 1000 m/s, $a/p = 0.5$ and for some values of $h/(2p)$.
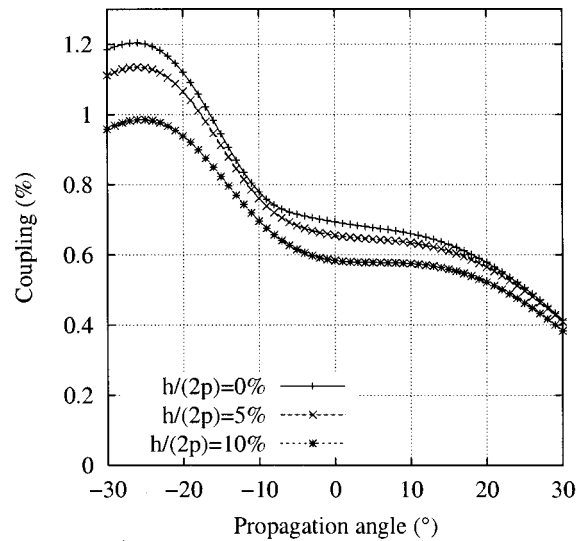

FIG. 10. Coupling strength of the SAW of X112°Y lithium tantalate in a periodic grating with $fp = 1000$ m/s, $a/p = 0.5$ and for some values of $h/(2p)$.

for comparison the case of a homogeneous layer of aluminum deposited on the substrate, with thicknesses equivalent to those of the gratings. The resonance slowness is seen to be rather strongly affected by the mass-loading effect, and to assume a symmetrical and mostly parabolic shape. The slowing down of the resonance velocity is mostly attributable to a sharp increase in the reflection coefficient per electrode. This behavior is quite different from what is usually observed in the first stop band, in which the slowing down of the SAW is much less effective. This is an indication that the reflection coefficient per period strongly depends on the excitation frequency. The beam steering remains limited, while the coupling increases with the propagation angle. It should be noted that no attenuation was found to occur at any angle.

The X112.2°Y, or $(XYt)/112.2$, cut of lithium tantalate is considered in Figs. 7–10. The dependence of the resonance slowness, beam steering, diffraction parameter and piezoelectric coupling for this cut are depicted in Figs. 7, 8, 9 and 10, respectively, for three values of the electrode aspect ratio $h/(2p)$ (0%, 5% and 10%), and again for an equivalent aluminum layer deposited on the substrate. The curves are not symmetrical around the 0° angle, as is expected for this cut without symmetry. Interestingly, it is seen that the velocity under a homogeneous aluminum layer is increasing with the thickness, while at the same time the velocity in the grating is decreasing. This is an indication that the slowness shift caused by the increasing reflection coefficient is the dominant effect.
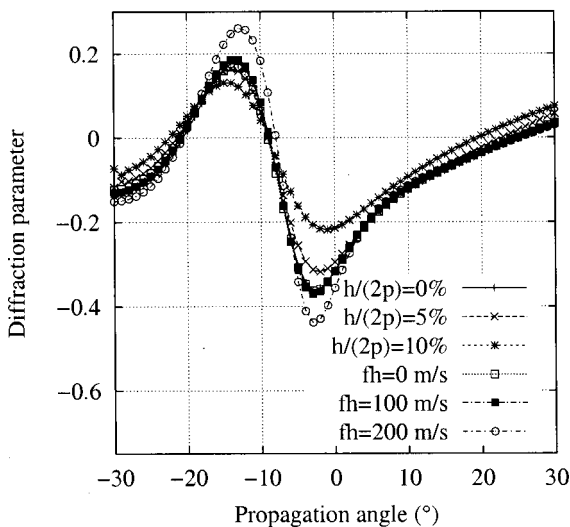

FIG. 9. Diffraction parameter of the SAW of X112°Y lithium tantalate under an aluminum layer for some values of fh, and in a periodic grating with $fp = 1000$ m/s, $a/p = 0.5$ and for some values of $h/(2p)$.
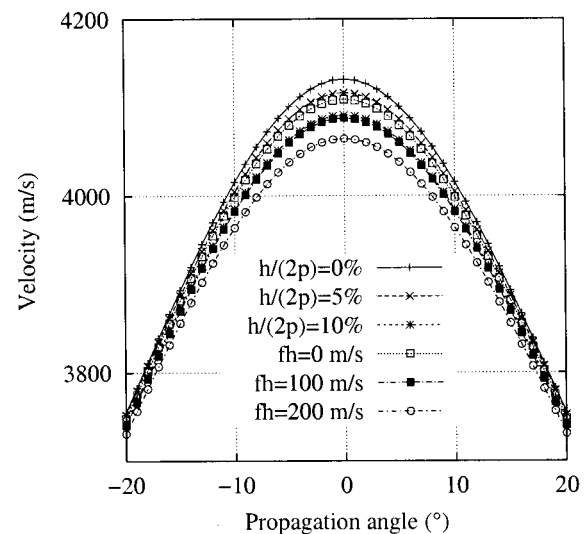

FIG. 11. Velocity of the leaky SAW of 36°YX lithium tantalate under an aluminum layer for some values of fh, and in a periodic grating with fp = 1000 m/s, $a/p = 0.5$ and for some values of $h/(2p)$.
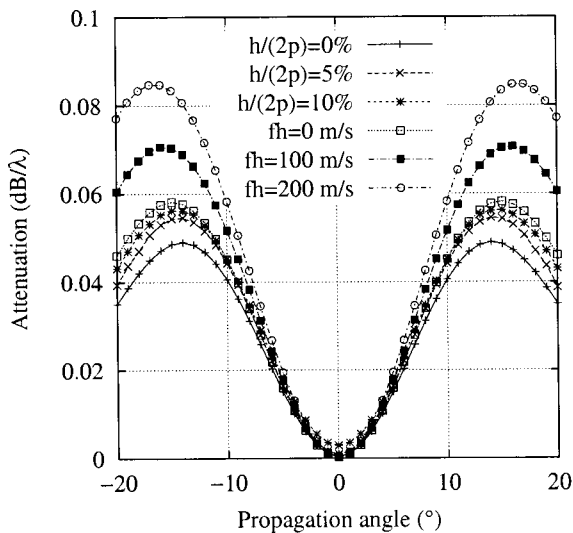
FIG. 12. Attenuation of the leaky SAW of 36°YX lithium tantalate under an aluminum layer for some values of fh, and in a periodic grating with fp = 1000 m/s, a/p = 0.5 and for some values of $h/(2p)$.

FIG. 14. Coupling strength of the leaky SAW of 36°YX lithium tantalate in a periodic grating with fp = 1000 m/s, a/p = 0.5 and for some values of $h/(2p)$.

The 36°YX, or $(YX\ell)/36$, cut of lithium tantalate is considered in Figs. 11–14. This cut is famous for its leaky, or pseudo, SAW. The dependence of the resonance slowness, attenuation, beam steering and piezoelectric coupling for the pseudo SAW are depicted in Figs. 11, 12, 13 and 14, respectively, for three values of the electrode aspect ratio $h/(2p)$ (0%, 5% and 10%), and again for an equivalent aluminum layer deposited on the substrate. The resonance slowness is seen to be much less affected by the mass loading effect than is that of the SAW of 42.75°YX quartz, but to assume a parabolic shape again. The beam steering varies rather largely with the propagation angle. The coupling is maximum along the grating axis, while at the same time the attenuation is at a minimum. As a consequence, in such a grating on $(YX\ell)/36$ lithium tantalate, the preferred direction of propagation is on axis; this is not the case for $(YX\ell)/42.75$ quartz.

As the above examples demonstrate, propagation under uniform films and periodic gratings are not comparable. This implies that diffraction models in which gratings are replaced by equivalent homogeneous metal layers should be systematically avoided, especially when extracting diffraction coefficients. Furthermore, when looking for minimal diffraction cuts, not only should the electromechanical properties of the substrate be taken into account, but also the actual thickness of interdigital transducers.

VI. CONCLUSION

The characteristics of surface acoustic waves propagating obliquely in electrode gratings have been investigated, with the mass-loading effect taken into account. The slowness of the surface waves, as well as the attenuation, piezoelectric coupling and beam steering have been obtained as a function of the propagation angle with respect to the grating axis. The method is based on the monitoring of poles in the harmonic admittance, which is computed using a FEA/BIM approach. A modification of classical finite element analysis was derived to account for slanted propagation. Examples were presented for 42.75YX quartz, X112.2Y lithium tantalate and 36YX lithium tantalate.
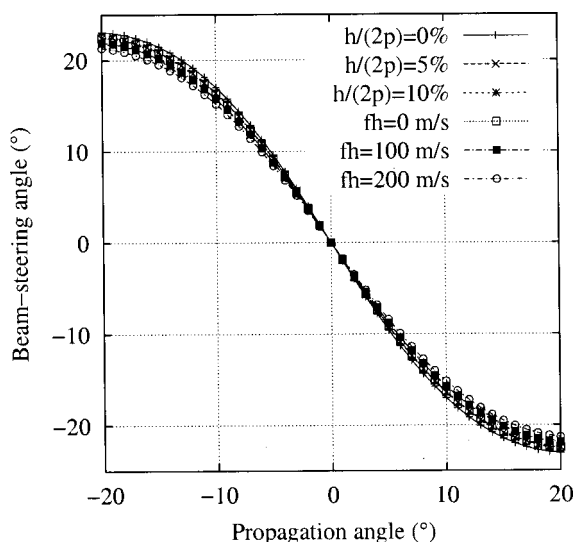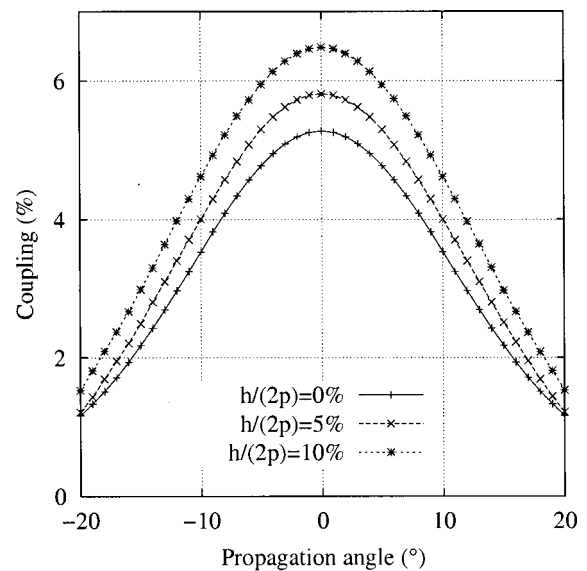
FIG. 13. Beam steering of the leaky SAW of 36°YX lithium tantalate under an aluminum layer for some values of fh, and in a periodic grating with fp = 1000 m/s, a/p = 0.5 and for some values of $h/(2p)$.

[1] R. Lerch, IEEE Trans. Ultrason. Ferroelectr. Freq. Control **37**, 233 (1990).
[2] M. Buchner, W. Ruile, A. Dietz, and R. Dill, in *Proceedings of the IEEE International Ultrasonics Symposium*, 1991, pp. 371–375.

[3] H. P. Reichinger and A. R. Baghai-Wadji, in *Proceedings of the IEEE International Ultrasonics Symposium*, 1992, pp. 263–266.

[4] P. Ventura, J. M. Hodé, and M. Solal, in *Proceedings of the IEEE International Ultrasonics Symposium*, 1995, pp. 263–269.

[5] G. Endoh, K. Hashimoto, and M. Yamaguchi, Jpn. J. Appl. Phys., Part 1 **34**, 2638 (1995).

[6] P. Ventura, J.-M. Hodé, J. Desbois, and M. Solal, IEEE Trans. Ultrason. Ferroelectr. Freq. Control **48**, 1259 (2001).

[7] G. Visintini, A. Baghai-Wadji, and O. Männer, IEEE Trans. Ultrason. Ferroelectr. Freq. Control **39**, 61 (1992).

[8] K. Hashimoto, G. Endoh, M. Ohmaru, and M. Yamaguchi, Jpn. J. Appl. Phys., Part 1 **35**, 3006 (1996).

[9] Y. Zhang, J. Desbois, and L. Boyer, IEEE Trans. Ultrason. Ferroelectr. Freq. Control **40**, 183 (1993).

[10] D. P. Morgan, *Surface-Wave Devices for Signal Processing* (Elsevier, Amsterdam, 1985).

[11] A. L. Slobodnik, E. D. Conway, and R. T. Delmonico, *Microwave Acoustic Handbook* (Air Force Cambridge Research Laboratories, Bedford, MA, 1973), Vol. 1A.

[12] R. C. Peach, in Ref. 4, pp. 221–225.

[13] K. Blötekjær, K. A. Ingebrigtsen, and H. Skeie, IEEE Trans. Electron Devices **ED-20**, 1133 (1973).

[14] E. L. Adler, IEEE Trans. Ultrason. Ferroelectr. Freq. Control **41**, 876 (1994).

[15] S. Datta and B. J. Hunsinger, IEEE Trans. Sonics Ultrason. **SU-27**, 333 (1980).

[16] O. C. Zienkiewicz and R. L. Taylor, *Finite Element Method* (Butterworth Heinemann, London, 2000).

[17] Proc. IRE **37**, 1378–1395 (1949).